Interface Roughness in Quantum Cascade Lasers

by
Kasparas Krivas

Supervisor: Prof. Andreas Wacker

Master Thesis

Division of Mathematical Physics, Lund University

Autumn semester 2014

LUND
UNIVERSITY

Abstract

The quantum cascade laser (QCL) is a solid state device capable of generating coherent mid-infrared and terahertz radiation. It is made from layers of different semiconducting materials. This layered structure gives rise to sub-bands, that are employed to achieve charge inversion necessary for lasing. However, the large number of interfaces, that are not perfect, strongly influences the operation of the device. In this work we study the influence of interface roughness (IFR) on the performance of the QCL. A program based on non-equilibrium Green's functions was used to simulated two realised terahertz lasers. These simulations provided current density dependence with respect to bias per period and the gain spectrum as well as the energetically and spatially resolved charge densities. The obtained data were analysed and compared with reference simulations in order to determine the dominant mechanisms by which the IFR scattering affects the operation of the QCL.

A number of phenomena were observed. One of them is the additive influence (superposition) of different interfaces on the current density. A shift or a decrease in an emission peak were also observed when interface roughness was altered.

By analysing the results, it was determined that interface roughness affects both current and gain of the investigated quantum cascade lasers. By investigating the spatially and energetically resolved electron densities, it was determined that one of the main mechanisms by which the IFR affects the operation of the QCL, is by electrons scattering into the lower energy sub-bands in the same well.

I would like to express my deep gratitude for my supervisor Prof. Andreas Wacker for his support, patients and constructed criticism during the course of the master thesis project.

Also, I would like to thank other members of the work group: Martin Lindskog, Josefin Reftlér and David Winge. I also want to thank the department of Mathematical Physics for a friendly atmosphere.

Contents

1 Introduction

Lasers are widespread used devices with applications in science (interferometry, spectroscopy etc.), industry (cutting, welding, tools of measurement or communication) and entertainment (laser shows). The quantum cascade laser (QCL) is a solid state device capable of generating coherent light which covers an important region of the electromagnetic spectrum (mid-infrared and terahertz radiation). This is the region poorly covered by other coherent radiation sources.

The first successfully operating device was demonstrated in 1994 by J. Faist [1]. It was recognised as a candidate for mid-infrared radiation. Therefore, QCLs attracted a lot of attention and were developed to the point that the mid-infrared lasers, operating at room temperature, can be used for industrial applications.

The quantum cascade lasers are based on semiconductor heterostructures, composed of hundreds of layers. Due to this complexity not all phenomena are well understood. One of them is the influence of interface roughness (IFR). It is known that IFR affects the QCL through elastic electron scattering, however, the precise way that the scattering influences the laser is unknown. However, as shown by C. Deutsch *et al.* [2], the IFR scattering is an important phenomenon that can strongly affect performance of QCLs.

The aim of this work is to investigate the influence of IFR scattering on the characteristics of current and gain of the QCL using the program documented in Ref [3]. The dominant mechanism of IFR scattering is to be determined from these results. The program is based on non-equilibrium Green's function theory (NEGFT). In this model IFR is described by the autocorrelation function with parameters η (root mean square (RMS)) and λ (correlation length). Interface roughness enters the simulation through self-energies Σ as the Fourier transform of autocorrelation function of interface spacial height distribution.

A two-well QCL [4] and a three-well QCL [5] were investigated. After comparing current and gain characteristics as well as charge and current density distribution, the importance of IFR scattering is assessed. In this way it is determined how IFR effects QCL operation.

2 Theory

2.1 Quantum cascade lasers

The principles of operation of quantum cascade lasers were first proposed by Kazarinov and Suris [6] in 1971. However, it took more then two decades until the first operating quantum cascade laser was manufactured by J. Faist [1] in 1994. Since then QCLs were recognised as promising devices that could be used to cover mid-infrared and terahertz frequencies. This is the electromagnetic spectrum range, that has a poor coverage by

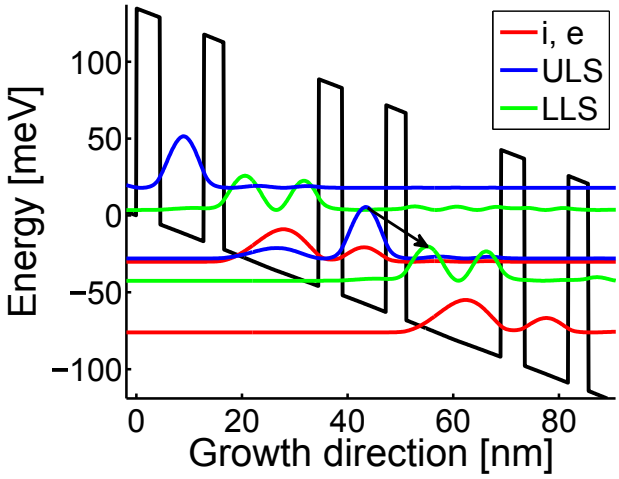

Figure 1: The band diagram of a simple quantum cascade laser, showing the lowest three states of two periods and the optical transition (black arrow).

other lasers.

To achieve lasing, population inversion must be created. This is a phenomenon, where a lot of electrons are stored in the quasi stationary higher energy state (upper lasing state (ULS)) while the lower energy state (lower lasing state (LLS)) is kept as empty as possible. This situation allows stimulated emission: a process where an electron drops from ULS to LLS, due to interaction with a photon. During this process another photon is emitted. The new photon has the same phase and energy as the initial photon. Therefore, coherent radiation is obtained.

There are several ways of creating population inversion. Most used is light pumping, when electrons are exited to the quasi stationary state by incoherent light source and later are transferred to ULS. However, being similar to solid state lasers, QCLs rely on electric pumping. This is a way of achieving population inversion by simply driving a current through the device.

2.2 Heterojunctions

To understand the advantages the QCL provides, the concept of a quantum potential well must be introduced. A quantum particle in a potential well is an important concept that has a lot of applications. This is one of the most important ideas that led to the design of the quantum cascade laser: a series of carefully designed quantum wells. While it is an easy task to model a single potential well and theoretically predict the features of a particle in it, it appeared to be much more complicated to manufacture one as discussed in Sec. 2.4.

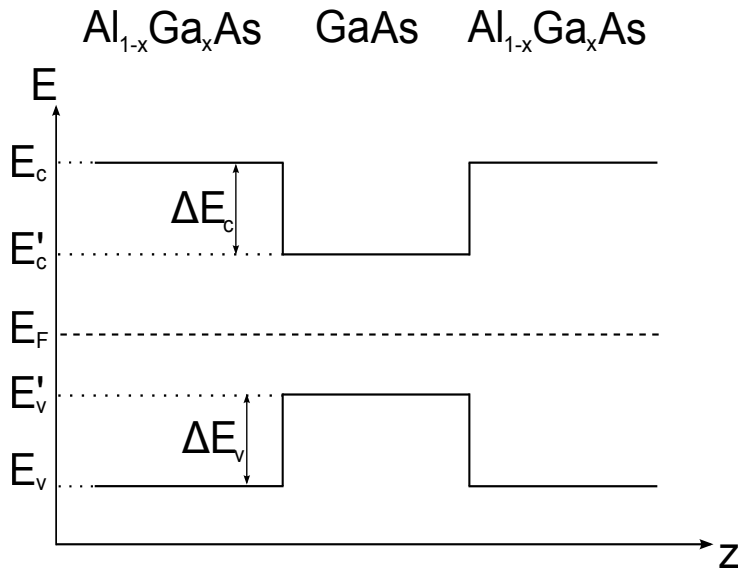

Figure 2: Diagram of a potential well in the conduction and valance bands. E_c and E_v are conduction and valance bands edges for the barriers (AlGaAs) while E_c' and E_v' are for the well (GaAs).

Semiconductor growth techniques allow to create crystals composed of different materials. The materials used (typical materials are GaAs and $Al_{1-x}Ga_xAs$) have different band gaps. However, since they are combined in a single crystal, the conduction band edge must be discontinuous. If the material with lower band gap (*e.g.* GaAs) is sandwiched between two layers of the large band gap (*e.g.* $Al_{0.85}Ga_{0.15}As$) materials, the potential well for electrons is formed in the conduction band as shown in Fig. 2. It can be seen, that a similar well is formed for holes in the valance band. However, holes have much higher effective mass than electrons and are rarely used to produce inversion.

As known from mathematical investigations of quantum wells, the particle placed in one of them will have quantized energy levels. The energy of these levels will depend on several parameters of the well: the width of the well, the width of the barriers and the height of barriers. The width of the well and the barriers can be chosen freely, but the height of barriers depend on the materials used. By adjusting these parameters, the energy levels can be changed, and this is exactly the feature used for tailoring the band structure of quantum cascade lasers.

However, until now we considered only one dimensional systems. In reality, by growing layers of different materials, one will achieve confinement in only one dimension. While in the growth direction electrons are confined and have strict energy levels, the movement in other directions will be unrestricted and will lead to the common dispersion law for a free particle. Of course this is an approximation, but the difference in confining is so huge (a typical well is several nanometres wide, while in-plane confinement is the same

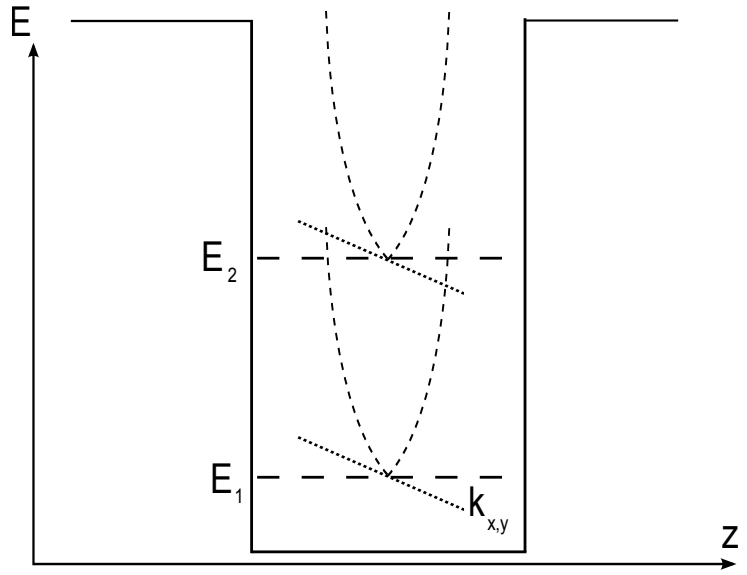

Figure 3: Diagram showing energy bands due to quantization as well as parabolas due to free motion perpendicular to the growth direction.

as the dimension of the sample, usually tens of microns), that particles can be assumed to behave as free particle perpendicular to the growth direction. This will result in a parabolic energy dependence (within the effective mass approximation) for motion in the in-plane direction. Therefore, the full energy of electrons can be expressed by:

$$E(z) = E_z + \frac{\hbar^2 k_\perp^2}{2m^*} \tag{1}$$

where E_z is the energy due to quantization in growth direction, $k_\perp$ is the in-plane momentum, $\hbar$ is the reduced Planck constant and m^* is the effective mass. This situation is depicted in Fig. 3.

2.3 Principle of operation

As opposed to conventional semiconductor lasers, where optical transitions happen between conduction band and valence band, QCL exploit sub-bands in the conduction band wells. In theory, the valance band could be also used. However, the much lower effective mass of charge carriers in the conduction band allows the easier control of operation. This is the reason why all current designs use the conduction band.

As described in previous section 2.2, the confinement in the growth direction gives rise to sub-bands that are used to guide electrons through the system. The QCL is composed of hundreds of identical periods. Each period is part of the main current flow through the structure. The main path for electrons is designed in such a way, that the electron would

participate in an optical transition. A single electron can create a lot of photons, and a high power can be achieved.

2.3.1 Terahertz QCL

"Terahertz radiation" is the commonly used term when referring to a frequency spectrum between 0.3 to 3 Thz. Despite high demand for applications, this region was poorly covered by coherent light sources. Earlier attempts to create lasers operating in terahertz frequency were of limited success. They suffered from various disadvantages. Lead salt lasers are made from rarely used materials, some other designs operated only at liquid helium temperature or required other extreme conditions. The possibility of tailoring quantum cascade lasers to operate at a specified wavelength allowed to create lasers overcoming most of former terahertz lasers problems. Being made from technologically mature material (gallium arsenide and aluminium gallium arsenide) these lasers have achieved the operation temperature of liquid nitrogen, Ref. [7]. The first quantum cascade laser operating in terahertz was demonstrated in 2002 by Köhler *et. al.* [8] and relied on chirped superlattice design. Currently, there are several active region designs for terahertz QCLs: chirped superlattice, bound to continuum and resonant phonon designs.

2.3.2 Resonant phonon design

One of the designs for active region used in terahertz quantum cascade lasers is the resonant phonon scheme. We will focus on this design, because it is the design of the laser investigated in this work. This set-up overcomes many problems of previous designs: how to have a high oscillation strength and an effective depopulation of the lower level. The high oscillation strength is required for effective lasing, while fast depopulation of the LLS is needed to maintain the inversion. Previous designs had two options: diagonal optical transition (a transition between states in adjacent wells) or vertical transition. The former design reduced the scattering from the ULS to the extractor state, however, it also reduced the ULS oscillator strength with the LLS. The later design had high oscillator strength, but a strong electron leakage from ULS by longitudinal optical (LO) phonons reduced the inversion.

As described in Ref. [9], the resonant phonon design achieves large oscillator strength and low LO-phonon scattering from the ULS. This is achieved by spatially separating the LLS and the extractor state. The electrons are transferred to the extractor state by tunnelling. This process is selective since the probability of electrons tunnelling into the extractor from the ULS is much lower. Electrons are then scattered by LO-phonons into the injector state. The selective depopulation strongly reduces the leakage from the ULS, but keeps the effective depopulation of the lower state.

2.4 QCL growth techniques

At the time QCLs were proposed, there was no technology to create such complicated structures. The reason why it took more then twenty years to produce the first laser is due to the large number of layers required for the laser to operate. In addition to that, the laser is extremely sensitive to fluctuations in the layers (wells and barriers) widths. If the layers are of a different width, then they are supposed to be according to the design, the sub-band structure will be altered and the electrons in this period will not behave as they are designed to.

In the 90s two epitaxy technologies were improved to reach the high enough precision levels to make these lasers. The main technologies that can be used for the QCL growth are molecular beam epitaxy (MBE) and metal organic chemical vapour deposition (MOCVD).

Despite the fact that crystals grow slowly for both of these methods, when compared to crystal growth techniques, there is still large amount of atoms hitting the surface at the same time. The places where atoms are deposited are randomly spread over all the sample surface and can not be controlled. Therefore there are several layers of the crystal growing simultaneously. As long as the bulk crystal is grown, this is not a problem. But when grown materials are changed (*e.g.* from GaAs to AlGaAs), this plays a significant role as one material mixes with another. This is the origin of the interface roughness scattering: there is no way of ensuring that all atoms deposited on the surface will be situated in the same layer. When the next material is grown, it occupies and fills all space between valleys, created by former material.

2.4.1 Molecular beam epitaxy

Molecular beam epitaxy (described in Ref. [10]) is the semiconductor growth process allowing to place layers of atoms one layer after another. This method allows to create the lowest concentration of impurities. The active zone is kept in ultra high vacuum. The materials (usually gallium, aluminium, arsenic, indium) for deposition are kept in Knudsen effusion cells. The source materials are then heated to high temperatures and begin to sublimate.

In the absence of any particles in the reactor chamber due to ultra high vacuum, the sublimed atoms travel to the sample without any collisions or interaction with other particles. This leads to high purity samples at the cost of growth speed, which is around one monolayer per second (1 μm per hour) as described in Ref. [11]. Due to the absence of any particles around the deposition site, this technique allows fast switching between growth materials to create interfaces of superior quality.

2.4.2 Metal organic chemical vapour deposition

Chemical vapour deposition is another growth technique used to grow high quality crystals, as described in Ref. [12]. It uses various metal organic compounds to carry atoms

into the reaction chamber. As opposed to MBE, this technique operates at a pressure of $0.1 - 1$ atm. It surpasses MBE for growth rates of bulk materials, but requires more time for switching between the growth materials.

The organic compounds used are metal alkyls (metal atoms with several groups of methyl or ethyl) and hydride molecules for non metal elements. These molecules are carried to the deposition site by hydrogen gas. Then the compounds are thermally decomposed and a chemical reaction occurs leaving non-volatile crystal and gases that are removed from the chamber. A simplified model, excluding all intermediate reactions, is a reaction between trimethyl gallium ($(CH_3)_3Ga$) and arsine (AsH_3). Gallium arsenide is formed after the reaction, while the residue atoms form methane which is flushed away by the stream of hydrogen gas.

2.5 Scattering in QCL

Scattering is an important phenomenon occurring in conductive materials. It is a process, where an electron changes its state due to some perturbation (weak potential). There are various scattering mechanisms in quantum cascade lasers, as described in Ref. [13]. These mechanisms also affect the electrons in different ways. There exists two types of scattering: the elastic scattering - when electrons change only momentum and inelastic scattering when both momentum and energy are changed. The elastic scattering mechanism are scattering from interface roughness and from impurities. Mechanisms attributed to inelastic scattering are spontaneous emission, phonon scattering and electron-electron interaction. It is also worth noting that during scattering events electrons can either be scattered from one sub-band to another, or the final state can be in the same band as the initial state.

All of these mechanisms are important for understanding quantum cascade lasers. Scattering affects the population of levels and the linewidth of the spectrum by reducing the lifetime of electrons in the sub-bands. The effect on sub-band population depends on the type of scattering. However, most of the times scattering reduces the lifetime of electrons in the band (thus enhances the current since electrons travel through the device faster). Electrons can form a leakage current by escaping the designated path by elastic scattering and thus therefore lowering the performance of the QCL. On the other hand, a well understood scattering phenomenon can be used in a clever way when designing QCLs, *e.g.* scattering by longitudinal optical phonons in resonant phonon design as discussed in Sec. 2.3.2.

2.6 Interface roughness scattering

The interface is a junction between two materials. When designing semiconductor devices, interfaces are considered to be perfect. However in reality they are not. Usually, the material from one layer gets into the other. This can be due to the fact, that during

the epitaxy process there are several layers growing at the same time. When materials are changed, the incomplete layers finish their growth with another material. This imperfection at the interface leads to an additional potential that affects electrons travelling through the crystal. Due to this interaction electrons can change their state.

The phenomenon when electrons change their state due to additional potential at the interface is called interface roughness scattering. It is an elastic scattering mechanism that changes only the momentum of an electron, but not its energy. During this process electrons can change bands and momentum, or just momentum. The event when electron stays in the same band does not have a lot of influence to the operation of the laser, since only current in the growth direction matters. The event when an electron changes band is the one that affects the QCL. Due to perturbation at the interfaces electrons can be scattered to different bands.

3 Model

3.1 Basis states

Bloch states are the most widely used states in describing solid bodies. However, they are spread over all the crystal. For purposes of numerical calculations, a set of localised states is desired. There is a way of using Bloch waves to construct a set of states that are localised over several wells. These states are called Wannier states. Here I sketch the method of constructing Wannier states (detailed derivation can be found in Ref. [14]).

Starting with the one dimensional Schrödinger equation for periodic heterostructure:

$$\left\{-\frac{\hbar^2}{2m_e}\frac{d^2}{dz^2}+V(z)\right\}\Psi(z)=E\Psi(z) \tag{2}$$

where effective mass m_e assumed to be constant over a material layer and $V(z)$ is the potential due to the heterostructure. This equation can be solved taking into account the periodical boundary conditions of the Bloch waves. The Wannier states can be written as a superposition of Bloch states:

$$\psi_\nu^W(z-nd)=\sqrt{\frac{d}{2\pi}}\int_{-\frac{\pi}{d}}^{\frac{\pi}{d}} e^{-inqd}u_q^\nu(z)dq \tag{3}$$

Where n labels the period, d is the width of the period and q is the momentum transfer. The sub-band index ν shows that a set of Wannier states is created for each sub-band. In fact, they are localised and there is one Wannier band in each period of the structure.

These equations depend on the phase of the Bloch functions. To maximise the effectiveness in the numerical calculations they should be as localised as possible. This can be achieved by fixing the phase of Bloch wave at some position. After testing several positions the optimal one is chosen.

As mentioned, there is single Wannier state, corresponding to the sub-band, in each period. Without external voltage these states are degenerate. However, when an electric field F is applied to the structure, the Hamiltonian used in Eq. 2 gets another term equal to $-eFz$. The new set of Wannier-Stark states solves the Schrödinger equation with the new Hamiltonian. These states can be written as the superposition of Wannier states. The Wannier-Stark states create ladders in space and energy, as shown in Ref. [15].

3.2 Model of the interface roughness scattering

To investigate the influence of interface roughness on the performance of quantum cascade lasers, a certain model of roughness must be created. The derivation of the following equations can be found in Ref. [14]. It is needed to assume some form of an interface. The assumption made in the model is that interface imperfections are wrong types of atoms introduced in the other material.

Interface roughness scattering in the Green's function model enters the equations through self-energies (a term that includes all interactions). By investigating Green's functions it can be seen, that interface roughness enters the self energies via the Fourier transform of the autocorrelation function for the spatial interface distribution. However, the form of the autocorrelation function is a matter of discussion, because no direct measurements have been performed. The two competing choices for autocorrelation functions are either a Gaussian distribution or an exponential distribution.

$$\langle f(\mathbf{r})f(\mathbf{r}')\rangle_g = \eta^2 \exp(-\frac{|\mathbf{r}-\mathbf{r}'|^2}{\Lambda^2}) \tag{4}$$

$$\langle f(\mathbf{r})f(\mathbf{r}')\rangle_e = \eta^2 \exp(-\frac{|\mathbf{r}-\mathbf{r}'|}{\Lambda}) \tag{5}$$

In this work, the exponential autocorrelation function was used. The Fourier transform of this function is:

$$f(q) = \mathcal{F}(< f(\mathbf{r})f(\mathbf{r}') >_e) = \frac{\eta^2\lambda^2}{(1+(q\lambda)^2)^{3/2}} \tag{6}$$

Thus, in Eq. 6 the parameters used to describe the IFR are η (the root mean square of displacement) and λ (correlation length). The variable q is defined as $q = \sqrt{q_x^2 + q_y^2}$ where $\vec{q} \equiv (qx, qy)$ is the in-plane momentum transfer.

This function enters the equations through self-energies Σ - which can be viewed as the additional energy of the particle due to interactions:

$$\Sigma_{\alpha\alpha'}(E, E_k) = \sum_{\beta\beta'} \int_0^\infty dE_{k'} \frac{\rho_0 A}{2} \frac{1}{2\pi} \int_0^{2\pi} d\phi \langle V_{\alpha\beta}(E_k, E_{k'}, \phi) V_{\beta'\alpha'}(E_k, E_{k'}, \phi)\rangle G_{\beta\beta'}(E, E_{k'}) \tag{7}$$

$$\Sigma_{\alpha\alpha'}(E, E_k) = \sum_{\beta\beta'} \int_0^\infty X^{\text{elast}}_{\alpha\alpha',\beta\beta'}(E_k E_{k'}) G_{\beta\beta'}(E, E_{k'}) dE_{k'} \tag{8}$$

$\alpha, \alpha', \beta, \beta'$ are the sub-band indexes, $X^{\text{elast}}_{\alpha\alpha',\beta\beta'}$ is the scattering matrix element, and $G_{\beta\beta'}(E, E_{k'})$ is the Green's function and $V_{\alpha\beta}(E_k, E_{k'})$ is the matrix element due to interface roughness scattering. The scattering matrix element part for interface roughness scattering with the exponential autocorrelation function Eq. 5 is written as [16]:

$$X^{\text{IFR}}_{\alpha\alpha',\beta\beta'}(E_k, E_{k'}) = \sum_j \frac{\Delta E_c^2 \eta_j^2}{2E_{\lambda_j}} \frac{1}{(a_j - b_j)\sqrt{a_j + b_j}} \Psi^{\alpha *}(z_j)\Psi^{\beta}(z_j)\Psi^{\beta' *}(z_j)\Psi^{\alpha'}(z_j) \tag{9}$$

The position (x_j) and IFR parameters (η_j and λ_j) are defined at the j-th interface, $\Psi(x_j)$ are the wavefunction values at the interface. The following shorthand notations are used:

$$a_j = 1 + \frac{E_k + E_{k'}}{E_{\lambda j}} \tag{10}$$

$$b_j = 2\frac{\sqrt{E_k E_{k'}}}{E_{\lambda j}} \tag{11}$$

$$E_{\lambda j} = \frac{\hbar^2}{2m\lambda_j^2} \tag{12}$$

3.2.1 Discussion of the influence of IFR

From Eq. 9, we can see that the transition probability increases as the wavefunction overlap increases at the interface. Considering that the effect takes place only at an interface, a significant overlap is required for the effect to be visible. Another important factor when assessing the influence of the IFR scattering is the occupation of bands. The effect gets stronger if there is a high electron density in one band and low density in another.

Interface roughness is an elastic scattering mechanism. This means that it changes only momentum, but not energy. Therefore electrons scattered by the interface roughness potential change only bands, but not energy. During the IFR scattering event electrons can escape the band in various ways:

- scattering to continuum
- scattering to higher energy bands in other periods
- change bands in the same well

The latest of these requires more attention since electrons scattered this way into lower energy bands will remain in the designated path. As can be seen in Fig. 4, the electron scattered elastically into another band can relax by emitting phonons. If bands are separated by large energy ΔE, it can take a long time for the electron to reach the lower states of the sub-band. Also, due to the lower occupation of states at high energies, the reverse process (scattering from lower band to upper band) will be weaker for bands with large separation in energy.

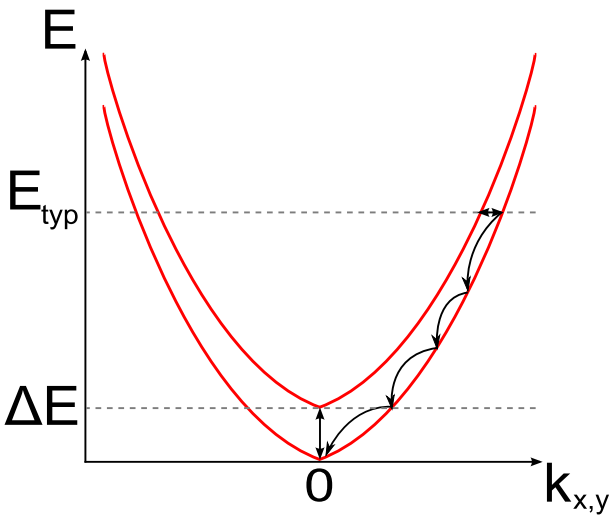

Figure 4: The elastic IFR scattering between two bands, separated by ΔE, followed by several relaxations by the phonon emission. In the approximation used in our program scattering happens at energy E_{typ} above upper sub-band edge.

3.3 Derivation of possible transitions

As described in Sec. 2.2, the energy of electrons in the nth band can be written as:

$$E_n(z) = \frac{\hbar^2 k^2}{2m^*} + E_n^\nu \tag{13}$$

Here ν is the period index, n is the state index, k is the in-plane momentum and E_n^ν is energy due to confinement in z direction and $E_n(z)$ is the total energy of electron in the nth sub-band with momentum k. It can be seen from Eq. 13 that bands are parabolic in k with their minima separated by some energy ΔE. In fact, each sub-band can be approximated as a paraboloid in k_x and k_y plane.

As stated in the previous section (Sec 3.2), the interface roughness scattering is elastic and can bring electrons from one band to another, or just change the state inside the same band. Since elastic scattering events that do not change bands hardly[1] influence current in the direction of interest (the growth direction), only the scattering events when electrons change the sub-band will be considered.

The sub-bands are separated in energy and momentum and scattering between sub-bands is restricted by available states. Due to this fact, for a given energy not all momentum transfer values are available.

Assuming that both bands are parabolas (as described in Eq. 13) with minima at

[1]Intraband scattering causes broadening

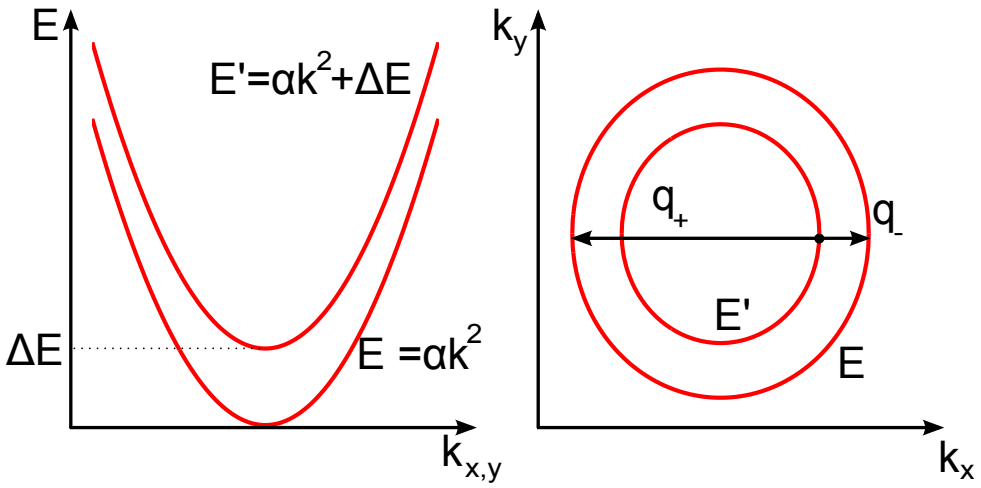

Figure 5: The dispersion law of two bands approximated as parabolas (*left*). Cross-section of two eliptic paraboloids at certain energy (*right*). The inner circle represents the parabola with minima higher in energy. The smallest and the largest possible transitions from the upper band to the lower band are shown.

$k = 0$ separated by ΔE, as shown in Fig. 5, one has

$$E = \alpha k^2 \tag{14}$$

$$E' = \alpha' k^2 + \Delta E \tag{15}$$

For elastic scattering, the energy does not change during the scattering event, so the calculated difference between parabolas is the possible momentum transfer. The momentum transfer (denoted $q = q(k)$) will depend on momentum k (and via the dispersion law on energy).

$$E(k) = E'(k - q) \tag{16}$$

Solving this equation yields

$$q_{\pm}(k) = k \pm \sqrt{ak^2 - b} \tag{17}$$

where a is the ratio between parabolicity coefficients $a = \frac{\alpha}{\alpha'}$ and $b = \frac{\Delta E}{\alpha'}$.

The parameter a can be approximated to unity. This can be justified by considering that the effective mass depends mostly on the distance from the valance band. Taking into account that the band gap for GaAs (the most common material for fabrication of the QCL) is $E_g = 1.52$eV (at $T = 0$K) and energy differences between sub-bands is in meV, it is easy to sea that the differences in effective mass will be negligible. Since the

parabolicity coefficients depend on the effective mass, the ratio between them can be approximated to be equal to unity.

As for all quadratic equations, there are two solutions. In this case one of them represents transition to the closer branch of other band, another - to the more distant branch.

However, as mentioned before, it must be noted that we are dealing with two dimensional elliptic paraboloids, therefore the allowed transitions are not only the branches $q_+(k)$ and $q_-(k)$, but also everything in between. The cross-section at a fixed energy is displayed in Fig. 5, where both parabolas at certain energy are shown as circles - the effective mass in both k_x and k_y directions is taken to be equal.

There is a minimum k value for the solution to exist, because for lower values the square root is imaginary. This can be easily understood by identifying that the square root becomes imaginary at energies, lower than the upper band minimum. As long as $ak^2 > b$, real solutions exist. The lowest energy scattering is with highest momentum transfer equal to:

$$q_\pm^2(k_0) = k_0^2 = \frac{2\Delta E m^* m_e}{\hbar^2} \tag{18}$$

Upon investigation we can see that the range between $q_+(k)$ and $q_-(k)$ is large. It would be useful to identify the region with higher density of possible transitions. To do that we first note that states are equally spaced in k-space. By looking in transition of $q(\phi = \pm\pi/2)$, we divide the outer circle in fig. 5 in half. By calculating the transition to these points we obtain the equation:

$$q(\phi = \pm\pi/2) = \sqrt{k^2(a+1) - b} \tag{19}$$

To obtain a better understanding of the function behaviour, we investigate the limit when k approaches infinity. At large k values, the solution approaches certain lines:

$$\lim_{k\to\infty} q_- = 0 \tag{20}$$

$$\lim_{k\to\infty} q_+ = 2k \tag{21}$$

$$\lim_{k\to\infty} q_{\pi/2} = \sqrt{2}k \tag{22}$$

From the equations above it is possible to see, that half of transitions are situated between 0 and $\sqrt{2}k$ and another half between $\sqrt{2}k$ and $2k$. So one half of transitions is distributed over the range $\sqrt{2}k = 1.41k$, and another over the range $(2 - \sqrt{2})k = 0.59k$. This means that the high momentum transfer in a possible transition range would be more sensitive to changes at higher q values in $f(q)$ (Fourier transform of autocorrelation function, Eq. 6).

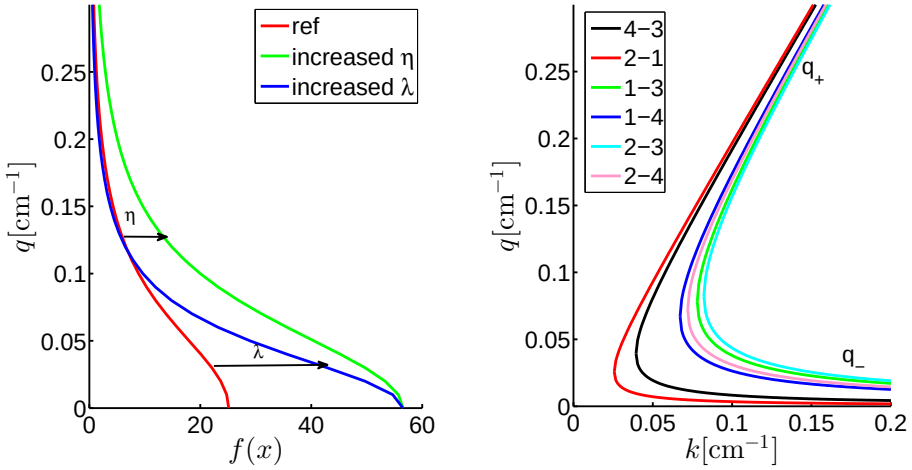

Figure 6: Fourier transform of autocorrelation function of the interface roughness spacial distribution as a function of q (*left*). Possible transitions between four bands in the three-well laser in Sec. 4.3 at operation bias of 57.5 mV per period (*right*).

3.4 The effect of possible transitions on QCL

As mentioned above, for certain k value, only the transitions between $q_-(k)$ and $q_+(k)$ are allowed. Both branches $q_\pm(k)$ for four separate bands are shown in Fig. 6 along with autocorrelation function. The black and the red curves are for bands separated by small energy difference. The sub-bands usually are filled to a certain level and all transitions between this level and bottom of the band are possible.

Here it must be noted, that the program uses a simplified model. To model scattering between two bands a certain energy E_{typ} is picked. This value corresponds to the energy at which the Green's function has a maximum. The value is chosen to simulate the thermal distribution and is written as:

$$E_{\mathrm{typ}} = E_{\mathrm{typ0}} + \delta E k_B T \tag{23}$$

E_{typ0} is the typical energy for 0K temperature, while δE is the slope of approximation. The values chosen are $E_{\mathrm{typ0}} = 7.4$ meV and $\delta E = 1$. As shown in Fig. 4, electrons are scattered from sub-bands at E_{typ} above the higher sub-band minimum. The scattering from the lower sub-band happens at the same energy as the scattering from the upper sub-band.

This type of approximation allows the faster computation. It can be argued that most of the scattering appear at this energy, so this approximation includes the larger part of transitions. Most of the simulations in this work were run for temperature $T = 200$ K. At this temperature the typical energy is $E_{\mathrm{typ}} = 23$meV.

Table 1: Typical ranges of possible momentum transfer, taking into account the E_{typ} approximation used in the simulations.

Case	ΔE[meV]	$[q_-, q_+][nm^{-1}]$
Small separation	5	$[0.008, 0.169]$
Medium separation	20	$[0.029, 0.190]$
Large separation	40	$[0.053, 0.213]$

Three distinct cases exist in the three-well laser. 1) bands are close to each other ($\Delta E = 2\text{meV} - 6\text{meV}$), 2) far from each other ($\Delta E = \ 40\text{meV}$) and 3) an intermediate case with $\Delta E = \ 20\text{meV}$. Typical ranges of possible transitions using E_{typ} approximation are shown in table 1.

Upon closer investigation of Fig. 6 and Table 1, it is clear that just some small part of the possible transitions can occur. It can be seen that as the band separation energy increases, the possible transition range shifts towards higher values.Therefore, it can be seen that the large momentum transfer q is more important for the sub-bands separated by a large energy.

4 Results

4.1 Two-well laser

The two-well quantum cascade laser is a laser produced by the ETH group [4]. It is one of the most simple laser designs possible. The period of this laser is composed of two wells. This QCL relies on three states - the lowest number of states needed for a QCL to work. Due to its simplicity it is a good design to check the influence of interface roughness.

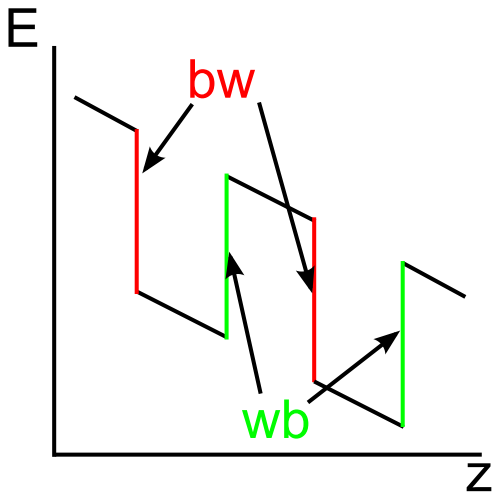

Figure 7: The conduction band edge (black line). The interfaces at the higher side of the wells (abbreviated bw) are shown in red, while the ones at the lower potential side of the wells (wb) are shown in green.

The band structure at operation bias is shown in Fig. 8. Electrons are injected in ULS from the injector-extractor (i-e) state. The transition between the ULS and the LLS is photon assisted (stimulated emission). Electrons are extracted from the LLS by longitudinal optical (LO) phonons. As can be seen from the Fig. 8, at operation bias (maximum current density) the injector-extractor state is in resonance with the ULS. This allows the fast transfer of electrons into the ULS and enhances inversion.

As mentioned above, this design employs longitudinal optical phonons to keep LLS empty. Phonons are quasi particles describing motion in the solid state lattice. Optical phonons arises when the primitive cell (smallest translational invariant unit in the lattice) of the crystal contains more than one atom. LO-phonons are of great importance in terahertz QCL. They are used for fast depopulation of the LLS. Another important property is that the large energy difference prevents thermal backfilling of the LLS. It is also worth noting that the energy of optical phonons in GaAs is higher than the typical energy that terahertz QCLs are radiating.

To increase inversion even further, the optical transition is realised in a diagonal way (the wavefunctions of the ULS and the LLS are localised in different wells, as can be seen in Fig. 8). Due to a thick optical transition barrier (3.8 nm), the overlap of the ULS and the LLS is low. This leads to a much lower transition probability and increases the lifetime of electrons in the ULS.

The reported laser structure, starting with barrier, is **4.5**/8.3/**3.8**/17.9. The doping is placed in the middle of the wide well, in a 5 nm wide region, having a sheet carrier density of $1.5 \times 10^{10}\mathrm{cm}^{-2}$. The material of the well is GaAs and the material used for barriers is $Ga_{0.85}Al_{0.15}As$.

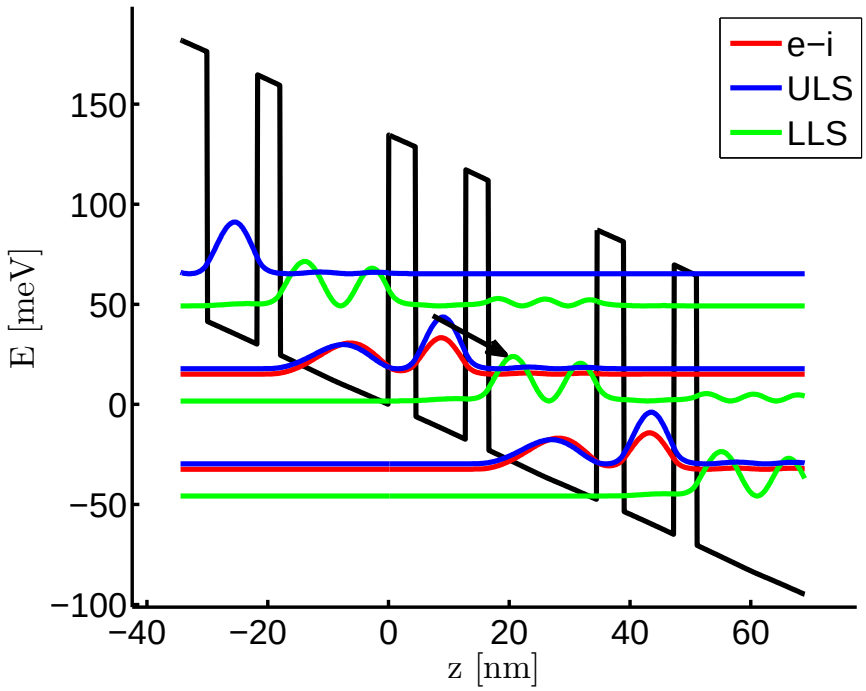

Figure 8: The sub-bands and the conduction band edge for the two-well design at operational bias of 47 mV per period. The optical transition between the ULS and the LLS in the central period is shown by arrow.

4.1.1 Influence of interface types

As described in Ref. [17], the interface roughness can depend on the direction of growth. Therefore, these simulations represent the case that occurs when real devices are made.

While there is no bias applied all wells are symmetrical. However, when bias is applied, the symmetry is broken as the potential energy on one side of the well becomes bigger then on the other side. This situation is shown in Fig. 7. The interface that is at the higher energy side of a well is abbreviated bw since, following the growth direction, a barrier is changed to a well. The interface at the lower side of the well is abbreviated wb.

It is known that a triangular form of the potential well leads to non-symmetrical states. The simple case of electric field effect on quantum well is described in Ref. [18], where a simple symmetric well is affected by an additional term arising from an applied bias. To describe a QCL, which is a much more complicated structure, one uses Wannier-Stark states, as described in Sec. 3.1. Due to the triangular form of the wells, these states are not symmetrical and are shifted towards the lower potential side of the well. This leads to higher overlap at the corresponding interface. Therefore one can draw an assumption, that different types of interfaces affect the operation of quantum cascade lasers in different

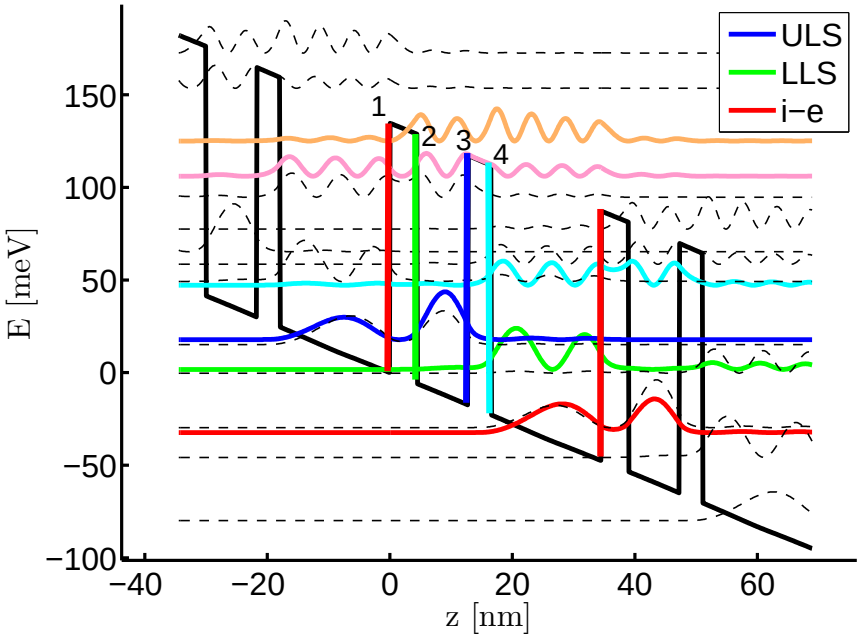

Figure 9: The sub-bands of the two-well laser. Interfaces are indicated by colours and numbers.

way.

First we investigate how roughness on different interfaces affects current of the QCL. To do that, 4 different simulations were run. The reference simulation was performed using the original interface roughness as described in Ref. [4]. Interface roughness for the other simulations was increased on certain interface types: two simulations with IFR increased on bw and wb interfaces separately and one with all interfaces having increased IFR. IFR values used are displayed in table 3.

The results are shown in Fig. 11 with increase in IFR realised as increase in parameter η. The first thing to be observed is that the increase in current is low compared to the absolute value of the current. The 50% increase in one of the parameters defining interface roughness scattering results in approximately 5% increase in current. This can be explained by noting that interface roughness scattering is just one of many processes happening in the QCL.

The next thing that can be seen is that wb interfaces affect current much more than bw. This can be explained by higher overlap at the respected interfaces. The wavefunction value at the interface tends to be higher for wb interfaces due to effectively lower barriers. The increase in current can be explained by enhancement of scattering between bands that allows electrons to travel through the system faster by reducing the lifetime of the bands.

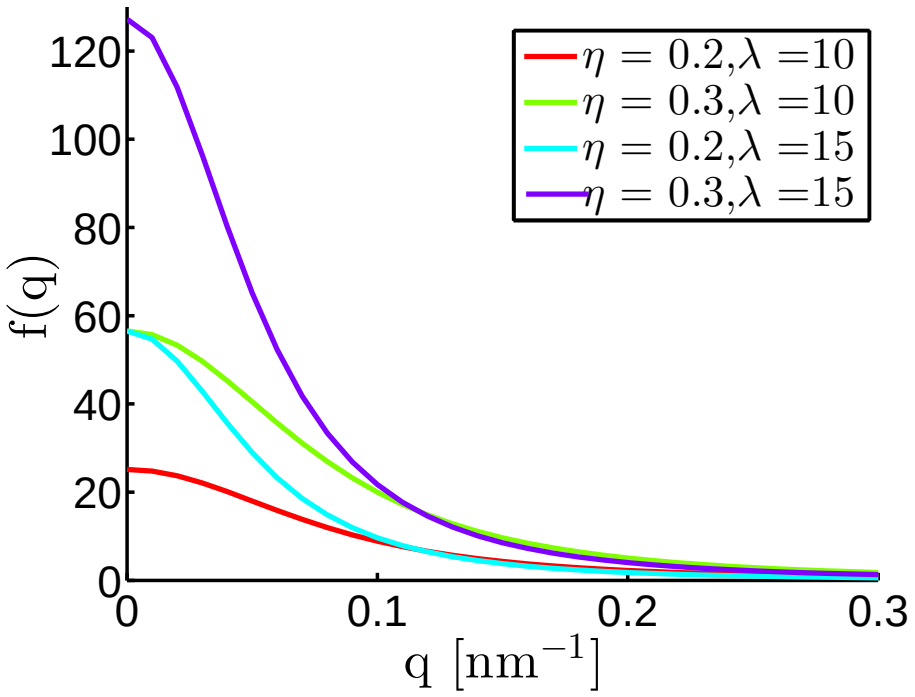

Figure 10: The autocorrelation function of interface roughness for different RMS - η and correlation length λ values.

Another phenomenon that is easy to see is the different peak in relative current. For wb type of interfaces the peak is shifted towards higher voltage compared to the bw case. This can be explained by the fact, that the wavefunctions shift to the lower energy side of potential well as bias is increased. This shift also increases the wavefunction value at the wb interface while decreasing the value at the other side of the well. Therefore, while initially (low voltage per period) the behaviour for separate types is similar (the wavefunctions are almost symmetrical), it starts to diverge at some point.

The last behaviour that is observed is the superposition of relative current. As shown in Fig. 11, the influence on current density from one type of interfaces can be added to the influence from another to get the values that are identical to the results obtained from all interfaces having altered IFR. This indicates that IFR effects are independent. The reason for this behaviour can be obtained from the occupation of bands. The changes in occupation can be obtained by extracting and comparing the number of electrons in various bands (displayed in Table 5) with the reference simulation. The change in bands occupation is small (usually less than 1%). This can explain the independent effects of separate interfaces on operation on QCLs.

The interface roughness is included in the model through the Fourier transform of the

Table 2: Normalised difference in electron number in bands (compared with reference).

band #	wb	bw	all
i-e	-0.95%	-0.82%	-1.77%
LLS	2.07%	-2.11%	-0.03%
ULS	0.01%	0.82%	0.83%

autocorrelation function of the spatial interface distribution $f(q)$ (Sec. 3.2). It can be seen that there exists two parameters that can be changed. The total of four distinct sets of parameters were used to investigate the influence of different interface types. The values are shown in Table 3 and the form of the Fourier transform of $f(q)$ is shown in Fig. 10.

Table 3: The set of parameters used to obtain different forms of autocorrelation functions of spatial interface distributions.

case	η [nm]	λ [nm]	abbreviation
#1	0.2	10	ref
#2	0.3	10	eta
#3	0.2	15	lambda
#4	0.3	15	all

As mentioned, the results shown in Fig. 11 are just for one of these sets. However, the same pattern was observed for the remaining configurations of IFR. All of them shown the increase in current density, stronger effect of wb interfaces and superposition of relative current density.

4.1.2 Influence of single interface

The investigation of the influence of a single interface can give an insight on the underlying mechanisms. There are different possibilities that IFR could affect the operation of quantum cascade laser: scattering to continuum,scattering to higher energy states or scattering into the other bands in the same period. Depending on the strength of each of these effects, IFR can either increase, or decrease the performance of the laser. Investigating a single interface allows us to understand which mechanism is the most important and why.

Three different sets of parameters, describing interface roughness, were used. They are shown in table 3 (the case when both η and λ were increased (labelled #4) is not used). The Fourier transform of the autocorrelation functions $f(q)$ for each set of parameters are similar to the ones shown in Fig. 10. It can be seen from Eq. 6, that at small momentum transfer q, $f(q)$ is approximately equal both for increased *eta* and increased *lambda* cases. The main difference is for larger q values, where *eta* effect is just a multiplication with

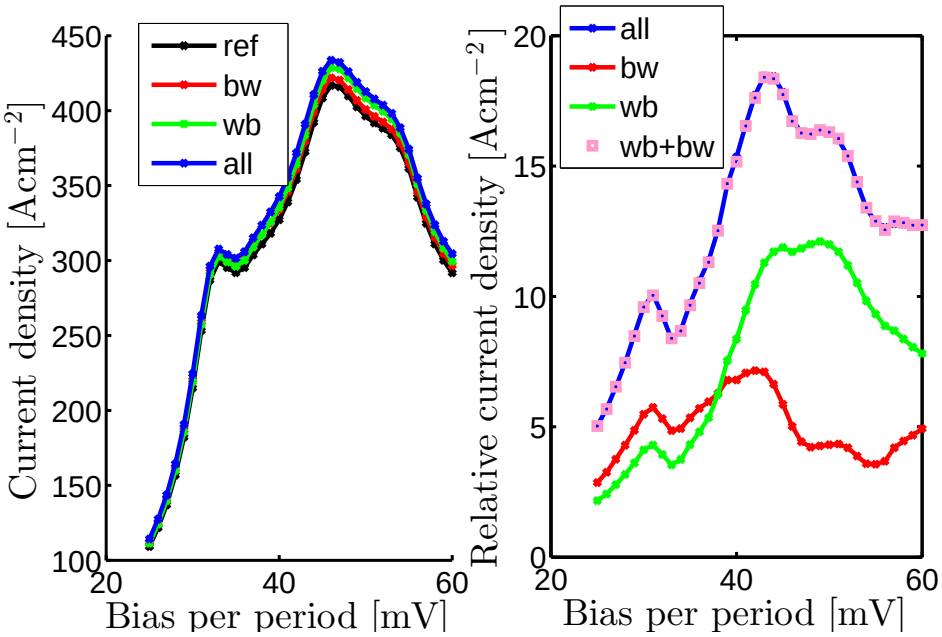

Figure 11: (*left*) Current density as a function of voltage per period. (*right*) Relative current of the three-well sample for wb-type, bw-type and all interfaces with increased IFR. It can be observed that the differences between summed values and the simulated curve is negligible.

Table 4: Interface roughness parameters used in two-well laser simulations.

case	η [nm]	λ [nm]	abbreviations
reference	0.15	10	ref
increased η	0.3	10	eta
increased λ	0.15	20	lambda

a constant, while *lambda* affects the $f(q)$ in much more complex way (at certain q value the function drops below the reference case).

To keep track of interfaces with altered IFR, the certain shorthand notation is introduced. Different numbers are assigned to the interfaces. The interface numbering is shown in Fig. 9. The injection barrier interface at higher potential energy is label 1, while at lower potential energy - 2, 3 is used for optical transition barrier interface with higher energy and the lower is given number 4.

The changes in gain are displayed in Fig. 12 for increased η case, and in Fig. 13 for increased λ case. It is clear to see that the influence on gain is similar for both cases. Therefore one can speculate that the absolute value of $f(q)$ describing IFR is of importance, not the form. It can be observed that the influence of the increased *eta* case

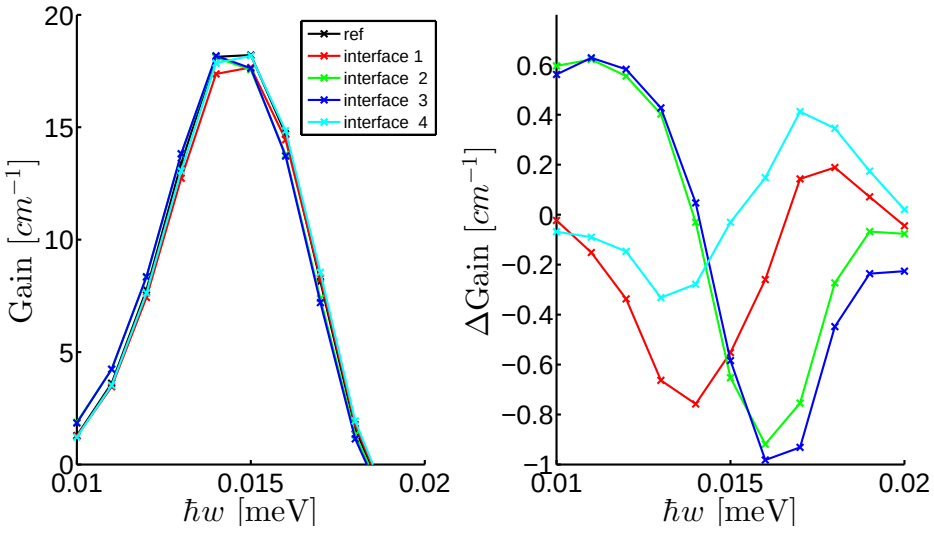

Figure 12: The simulation results for two-well laser with IFR on one interfaced altered to have increased *eta*. (*left*) Gain spectrum, (*right*) change in gain (compared to reference simulation).

is higher. This can be related to $f(q)$ being higher in this case for all values of momentum transfer.

The other thing to be observed in the gain spectrum is a shift in peak value. It can be seen that the shift direction depends on the well, in which the interface with altered IFR is located. The interfaces labeled 2 (green line) and 3 (blue line) are in the well where the wavefunction of the ULS has a maximum. Increasing IFR on one of the interfaces in this well leads to the red shift - gain peak shifts to lower energies. On the other hand the interfaces in the wide well: 1 (red line) and 4 (cyan line) shifts peak to the higher energies - a blue shift is observed. This tendency is common for both cases: increased η and increased λ.

One of the possible explanations for the observed gain behaviour can be the obtained by investigating the self-energies influence on the energy of the sub-bands. One of the results of the second order perturbation theory (as can be seen from Eq. 24 below) is that the energy of the ground state is always reduced as a perturbation increases. Therefore by increasing IFR (perturbation potential) the ground state energy in the well is decreased.

$$E_n^{(2)} = \sum_{k \neq n} \frac{|\langle k^0 | V_{\text{pert}} | n^0 \rangle|^2}{E_n^0 - E_k^0} \tag{24}$$

Increasing energy in the well with the ULS will cause the red shift, since the ULS is pushed down and the optical transition energy is lowered. The blue shift is observed if IFR is increased in the well with the LLS, since in this case the difference between

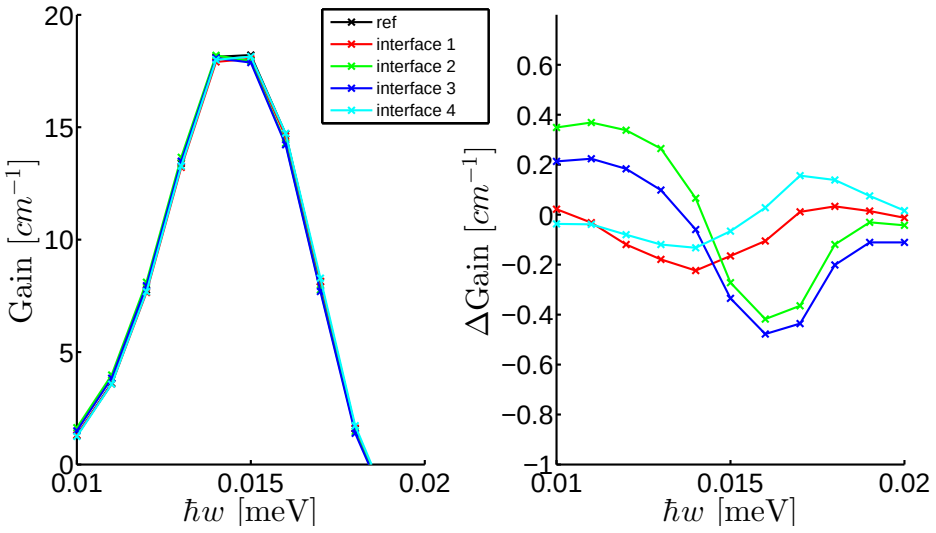

Figure 13: The simulation results for two-well laser with IFR on one interfaced altered to have increased *lambda*. (*left*) Gain spectrum, (*right*) change in gain (compared to reference simulation).

the ULS and the LLS increases. The discussion will be continued when investigating the three-well laser in Sec. 4.5.

The next stage is to try to understand the physical processes that lead to this kind of behaviour. Some insight can be obtained by examining the resolved electron densities and taking into account possible transitions as described in Sec. 3.4. However, extracting information directly from the resolved electron density is nearly impossible. This is due to the fact that changes in the local electron densities are really small: usually two, or more, order of magnitude lower than the value. Therefore a difference between simulations with changed IFR and the reference sample is investigated instead, as shown in Fig. 14.

It is easy to observe that just as in the gain case, the behaviour is similar when interfaces are altered in the same well: relative densities for interfaces Nr. 2 and 3 look very similar, just as for pair the 1 and 4. It can be observed in Fig. 14 that there are zone with increased electron number at higher energies. This indicates that electrons are scattered from the upper levels into the lower levels and then relaxes by phonon emission as shown in Fig. 4.

4.2 Convergence check

Every numerical approach introduces errors into the solution. The main source of this discrepancy with an analytic solution are truncation errors and the methodical errors. The truncation error is the error made by truncating numbers stored in floating point

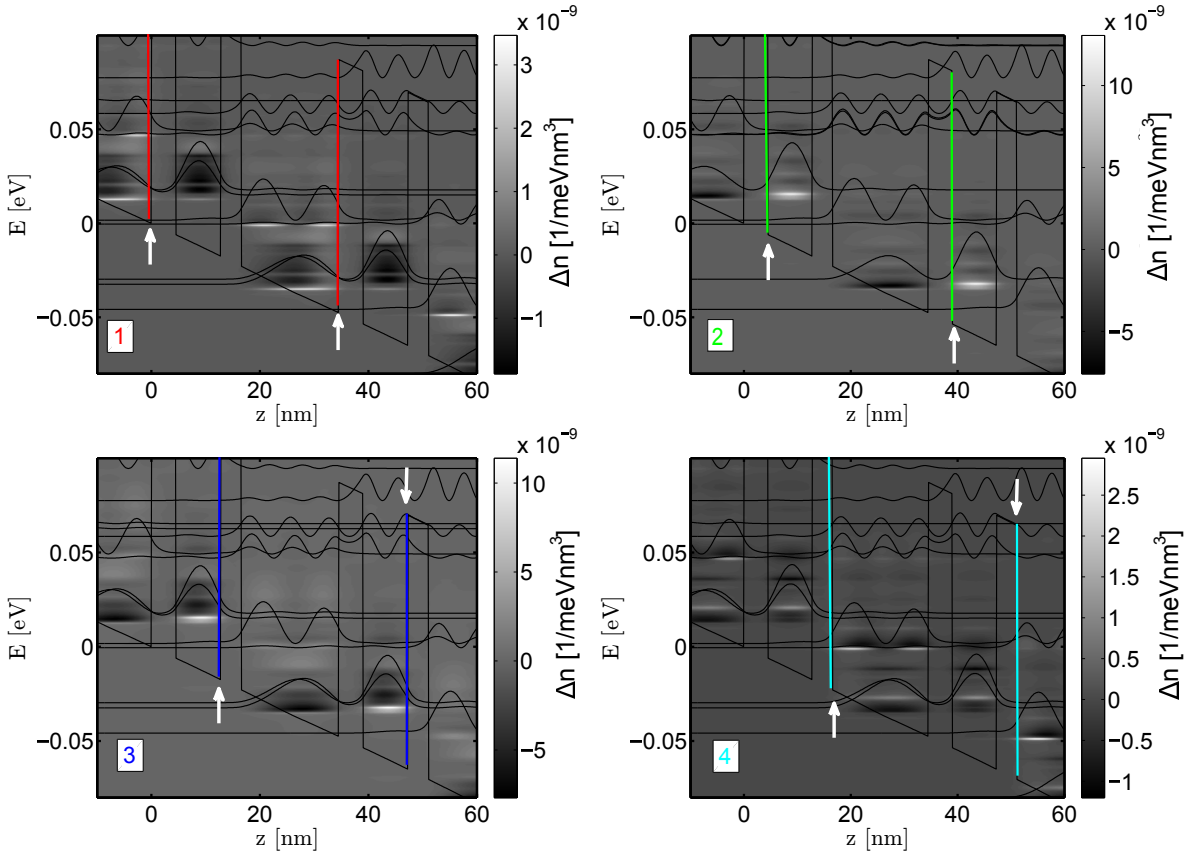

Figure 14: Relative electron density (compared to the reference sample) resolved in energy and growth direction (z) for four different positions of the interface with increased η. Positions of altered interfaces are indicated by coloured lines (the influence of these interfaces is shown in Fig. 12 and Fig. 13). Results were obtained at a bias per period equalt to 46.5 mV.

format. These numbers can not be stored in the finite amount of memory and must be truncated at some point. This introduces the error that is unavoidable.

Another kind of error is introduced by the use of a numerical calculation method. This error is due to the discretisation of continuous variables. In the program used for QCL modelling, energy and momentum spaces are discretised. The discretisation is defined by two parameters: n_e - discretisation of energy, and n_k - discretisation of momentum space. There is also the convergence criterion δ_{konv}, which determines the minimum convergence the solution must reach before it can be considered as non-changing. These parameters define the resolution of the grid used for calculations and the precision of the obtained solution. However, there are other parameters that effect the resolution through the range of energy needed for calculations (*e.g.* maximum bias).

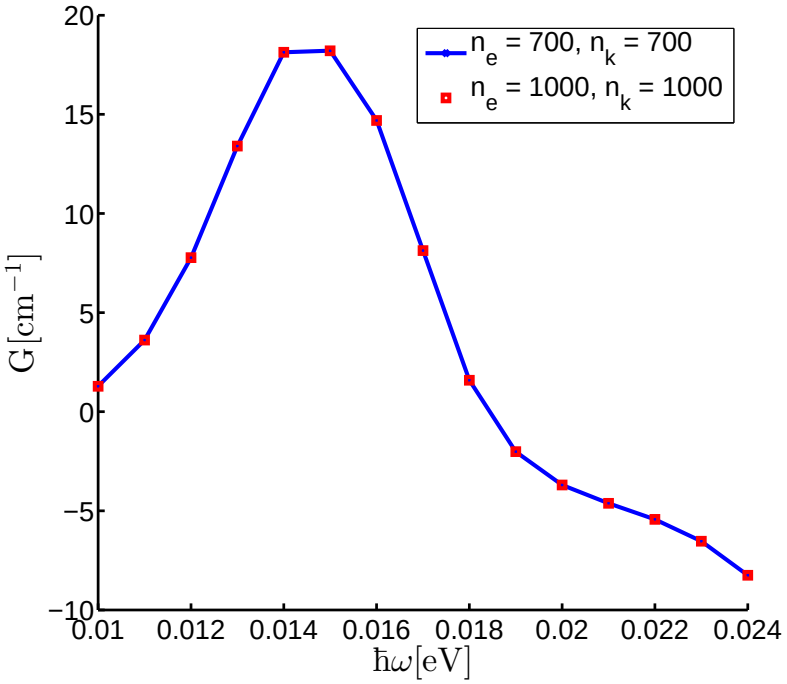

Figure 15: Convergence check for two-well laser. The difference in results with two different sets of precision defining parameters is negligible.

Due to complexity of the program it is nearly impossible to estimate the errors in an analytic way. However, there is a way to ensure that results are reliable. The way is to ensure the numerical convergence of the results. Better convergence is achieved for higher resolution of dicretised variables. Therefore, if an increase in discretisation parameters and convergence criterion do not change the results, one can assume that results are trustworthy.

The convergence check was performed by increasing the energy discretisation from n_e = 700 to 1000 and n_k from 700 to 1000. Also the convergence criterion was increased from $\delta_{\text{konv}} = 5 \cdot 10^{-4}$ to $1 \cdot 10^{-4}$. The results are shown in Fig. 15. It is easy to observe that results for lower resolution and worse convergence were almost identical to the results of the higher precision simulation.

Therefore, it is possible to conclude that the set of parameters $n_e = 700$, $n_k = 700$ and $\delta_{\text{konv}} = 5 \cdot 10^{-4}$ is good for obtaining reliable data. All simulations for the two-well laser were performed with these parameters.

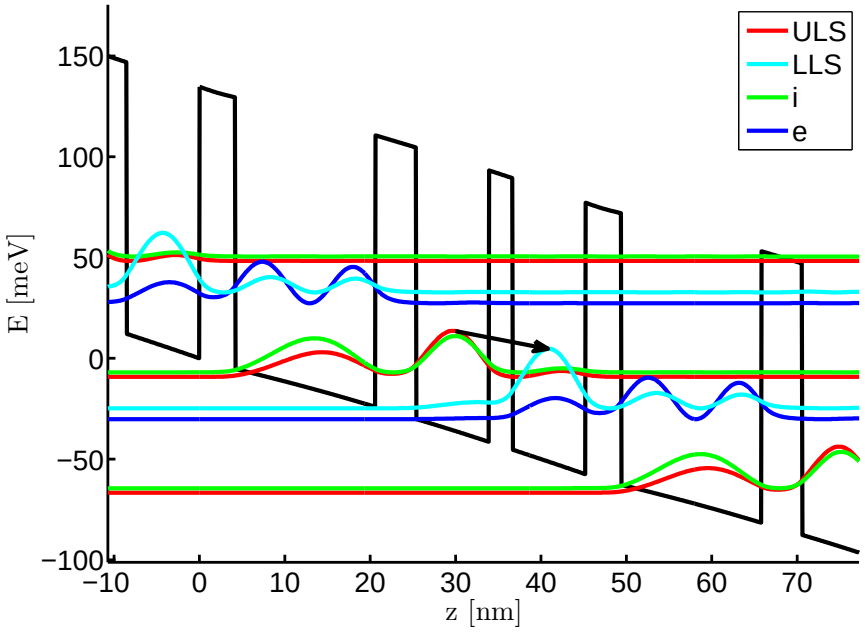

Figure 16: The sub-bands and the conduction band edge for the three-well design at operational bias of 57.5 mV per period. The optical transitions between the ULS and the LLS in the central period is shown by the arrow.

4.3 Three-well laser

Another QCL design that was chosen for the interface roughness study is the three-well quantum cascade laser by Kumar *et. al.* [5]. It is a resonant-phonon (Sec. 2.3.2) design that relies on 4 bands to carry electrons through the structure. It was demonstrated that this device can operate at temperatures higher than liquid nitrogen. Technical data of this laser is shown in Appendix A Table 8.

This laser structure, as documented in Ref. [5], is **4.8**/8.5/**2.8**/8.5/**4.2**/16.4, starting with an injector barrier. The 4.2 nm wide barrier is delta doped (dopants are placed in a thin layer) with $3 \times 10^{10}\text{cm}^2$. This laser has four state that are necessary for laser operation: upper lasing state (ULS), lower lasing state (LLS), injector (i) and extractor (e). These four Wannier-Stark states of three periods are shown in Fig. 16.

The optical transition is diagonal. That means that overlap between the ULS and the LLS is small to increase the lifetime of electrons in the ULS. This in turn increases the inversion, which is needed for effective QCL operation. To keep high inversion, the electrons must be removed from the LLS effectively. This is achieved by resonant tunnelling to an extractor state: the LLS and extractor states have almost the same energy at operating bias and electrons can change between them easily. The extractor state is spread

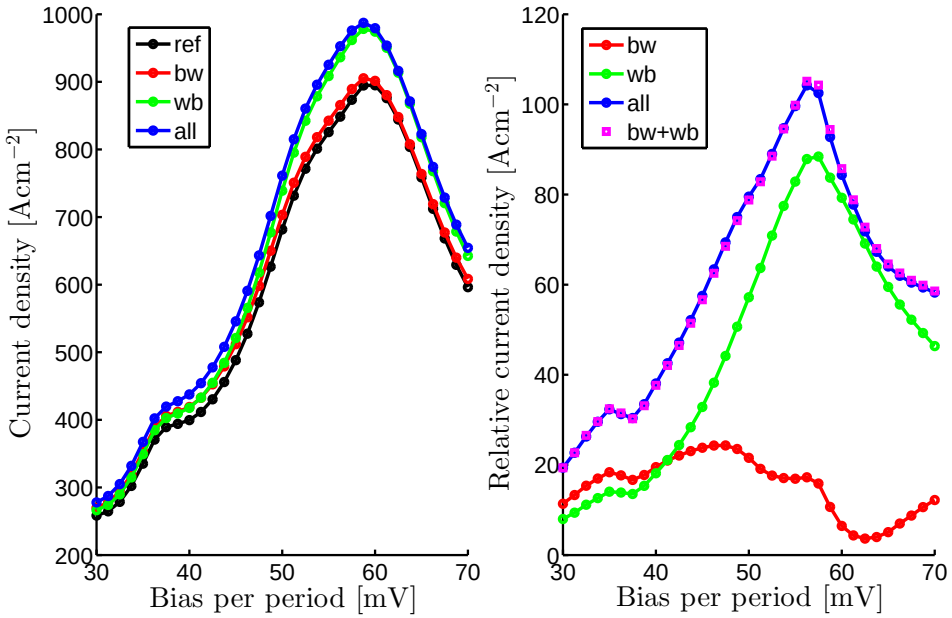

Figure 17: (*left*) Current density as a function of bias per period for the three-well QCL. (*right*) Relative change in current density (compared with the *ref* sample, described in table 6) as a function of bias per period.

over several wells and electrons scattered from LLS into an extractor state are carried to further wells. In wide well, at operation bias, the energy difference between extractor and injector is equal to the longitudinal optical (LO) phonon energy. This allows the fast electron scattering between these states by LO phonons. The injector state has the large overlap with the ULS. Electrons are then scattered into ULS and repeat the cycle in the next period.

Since there are 222 periods, each electron could produce a large amount of photons. However, it is clear that part of the electrons do not follow an ideal path due to the scattering mechanisms. The influence of IFR scattering is therefore investigated here.

4.4 Influence of interface types

The investigation of the three-well laser follows the same pattern as for the two-well laser. The first step is to check the current dependency on changes of IFR for one type of interfaces. The interfaces types were labelled as bw for the higher potential side of the well and wb for the lower side, as shown in Fig. 7. The results for current when parameter η in $f(q)$ Eq. 6 was changed are shown in Fig. 17.

It can be observed that the current is increasing when the interface roughness is

Table 5: Change in electron densities for the first four bands for different IFR configurations.

sub-band	wb	bw	all
ULS	1.7%	-0.3%	1.5%
injector	-0.2%	-2.1%	-2.3%
extractor	-0.4%	5.1%	4.6%
LLS	-3.3%	2.3%	-0.9%

increased. This is because the increase in corresponding scattering drives the electrons through the structure faster. By comparing the current density plot (Fig. 17 (*left*)) with the corresponding plot of the two-well laser in Fig. 11, we can observe that the three-well laser is more sensitive to changes in IFR.

A much larger increase in current is observed for the wb case. The reason for this effect is the fact that sub-bands wavefuntions overlap much more at lower side of the well. The wavefunctions have much larger values at the mentioned interfaces, increasing as the bias is increased. The fall in the following the peak can be explained by noting that the operation bias for this laser is around 57 mV per period. At larger biases, the sub-bands misalign and the current drops.

Also, there exists a shift in relative current peak, just like in the two-well laser. Interfaces at the higher potential side (bw) affect the current more for lower biases, and interfaces at lower potential energy side (wb) of the well affect more at higher biases. This can be attributed to higher overlap at corresponding interfaces. The higher overlap at wb interfaces follows from relatively higher energy at these interfaces compared to the conduction band edge than at the other end of the well.

Another phenomenon is the superposition of relative currents. This could be explained by low changes in the occupation of the sub-bands. The change in electron densities in four bands can be seen in Table 5. However, it can be seen that at some cases electrons are redistributed in the bands. While electron population in the extractor state increases a lot (up to 5.1% in bw case) it can be argued that this state does not play any critical role in electron transport through the structure, because the 'bottleneck' of the system is the transition between the ULS and the LLS. It can be observed that occupation of these states are changed less.

4.5 Single interface simulations

Just as in two-well laser case, the single interface influence to the operation of QCL should provide a lot of insight of the underlying phenomena. It was observed that due to more complex scheme and greater number of interfaces the influence of IFR is higher for this laser than it is in two-well laser case. There are three barriers in each period. They can be named by their function: injection barrier, optical transition barrier and extraction

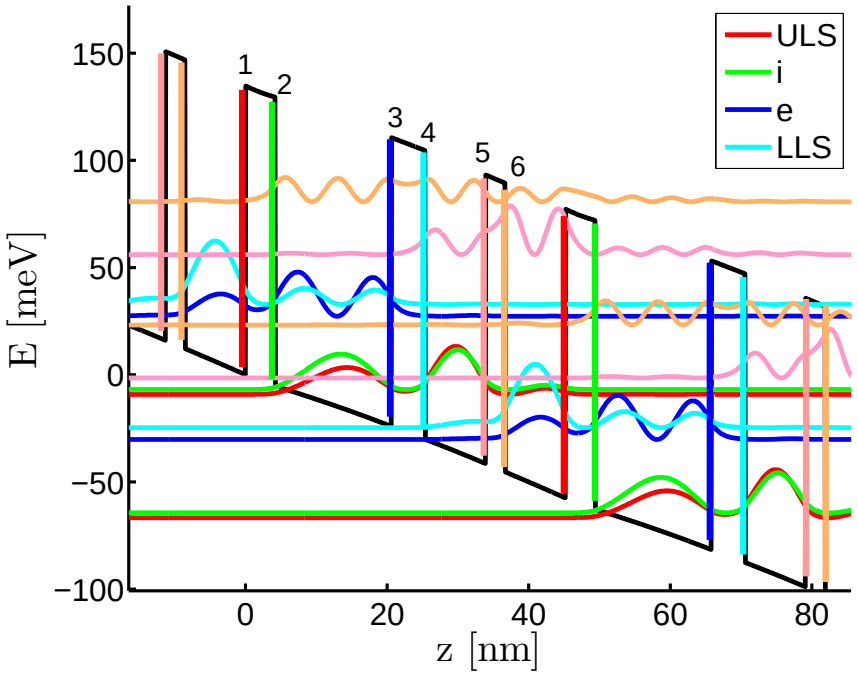

Figure 18: Band diagram with wavefunctions of the middle period. Colours and numbers indicate the interfaces. The optical transition between the ULS and the LLS is shown by arrow.

barrier. Each barrier has two interfaces. After bias is applied to the structure, one of them is elevated in potential energy scheme in respect to other, therefore breaking the symmetry. The interfaces can be labelled using numbers: staring with the extraction barrier interface with higher energy, as shown in Fig. 18.

Three sets of parameters determining the Fourier transform of the interface roughness autocorrelation function were used in these simulations. They can be found in Table 6. The reference sample was the one with all interfaces having *ref* IFR, while increased η and λ simulations have one specified interface with corresponding altered interface roughness.

As mentioned above, the band structure of a three-well laser is much more complex than the structure of the two-band QCL. The first thing to note is that there are various places in the design of this QCL where elastic scattering due to interface roughness is possible (high wavefunction overlap at interface) and possibly harmful for operation (possible leakage of electrons).

The results for the difference in gain are shown in Fig. 19. The first thing to notice is a shift in gain peak for most of the cases. Also it is worth noticing that interfaces on the lower potential energy side of the well have stronger negative effect on gain than their counterparts on the higher potential energy side of the well.

Table 6: Interface roughness parameters used in three-well laser simulations.

case	η [nm]	λ [nm]	abbreviations
reference	0.20	10	ref
increased η	0.3	10	eta
increased λ	0.20	15	lambda
increased all	0.30	15	all

4.5.1 Wide well (injector-extractor well)

Upon investigating Fig. 19 one can see that the interfaces labelled 2 and 3 (interfaces in the injector well) affect the gain least.

The effect of the interfaces in cases 2,3 and 6 is a shift in the gain peak. The three-well laser displays a similar response to the increase in IFR as can be seen by comparing Fig. 19 with Fig. 12 and Fig. 13. The shift can be understood using the same explanation as in Sec. 4.1.2. The increase in perturbative potential increases the self-energies. Due to the increase in the real part of self-energies, the energy levels are shifted (ground state is always shifted to lower energies). The lower lasing state being shifted to lower energies would result in blue-shift, just as it is observed in relative gain plots.

Note, that there exists a non-zero value of the LLS and extractor states wavefunctions at both interfaces (however, the values are higher at the wb interface). Therefore at these interfaces the large momentum scattering could decrease gain, due to electron loss from the ULS and injector states. The fact that the possible momentum transfer q range is wide should be also take into consideration. The large q values effect the scattering between bands with large energy separation more. Therefore we can expect that IFR with increased η will give worse results then when λ is increased (since this type of IFR favours low momentum transfer scattering).

In the wide well of this structure, electrons are supposed to be scattered by the LO (longitudinal optical) phonons from the extractor state to the injector. The energy difference between these bands is the largest (compared with the other differences in the designed electron path). This leads to high momentum transfer values needed for the elastic scattering between these bands. The effect of elastic scattering is not easy to estimate, because electrons that are scattered by IFR end up in the band they were suppose to (injector), however, at higher energies. These electrons later relax by emitting phonons. Therefore it takes more time for these electrons to reach bottom of the sub-band, however, the electrons in injector (despite being in higher energy states) can continue the designed path. This process can be seen in Fig. 20 as whiter regions (increase in electron density).

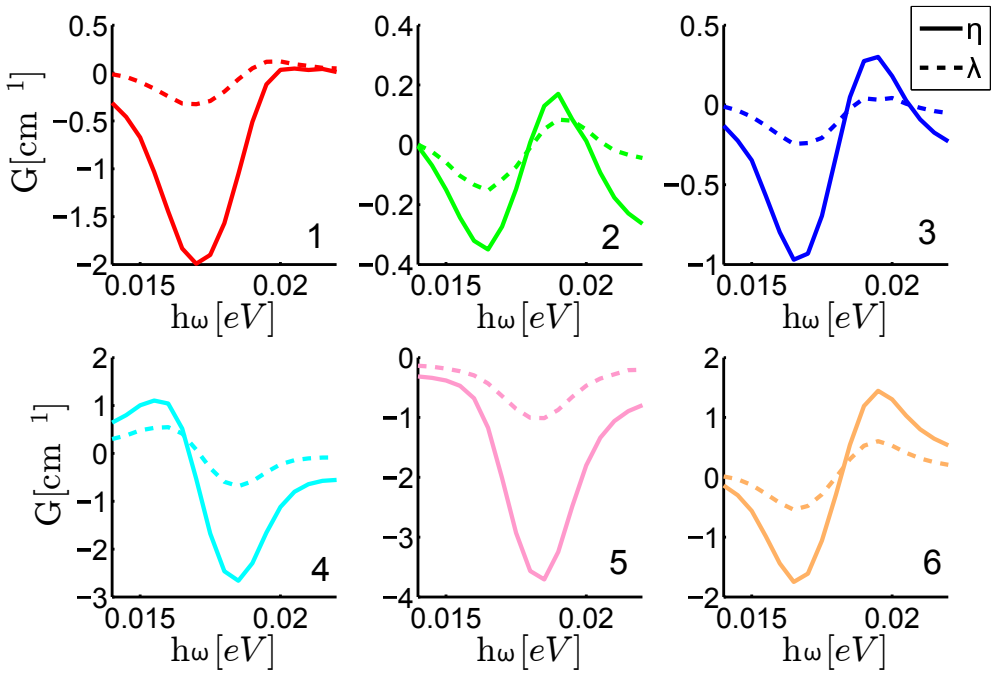

Figure 19: Difference in gain for different interfaces. Solid lines shows results when η is increased, dashed lines - when λ is increased. Colours indicates different interfaces and are shown in Fig. 18. Simulations were performed at 57.5 mV bias per period.

4.5.2 Upper lasing state well

The interfaces in this well are labelled 4 and 5. This is the well with ULS having its maximum. Similar well exists in two-well design (Sec. 4.1.2). However, in this case we can notice a strong decrease in gain, especially in interface 5 case.

The interface 5 shows steady loss in gain: for all frequencies and for both autocorrelation function $f(x)$ forms. That demonstrates that leakage from the upper state to the lower happens not only due to large momentum transfer values, but also due to small (that can be seen for increased λ). The much stronger negative effect compared to interface 4 can be attributed to a higher overlap at the interface. The higher overlap is due to the fact that the effective barrier height is diminished due to the applied bias and that the wavefunctions are shifted towards the lower energy interface.

It is possible to notice some red-shift. However, due to the strong decrease in gain the shift in peak is not apparent. Just as in two-well laser case, red-shift in this well can be explained by the decrease in energy of the ULS, caused by increased IFR.

The shift can be easily seen for interface 4 when λ is increased. That suggests that the large decrease in gain is due to electron loss from the upper pair of sub-bands in energy

(ULS and injector states) to the lower pair (LLS and extractor). The mechanism of this loss is shown in Fig. 4. Electrons are scattered elastically into the sub-bands with much lower energy at minimum and then relaxes by the phonon emission.

Since the population inversion is created between the ULS (that has maximum in this well) and LLS (that has maximum in the next well), this well exhibits strong dependence on IFR scattering. The increase in IFR results in electrons leaking from ULS to the LLS. This leakage strongly decreases the gain.

4.5.3 Lower lasing state well

In the lower lasing state well (interfaces 1 and 6) a blue-shift is observed. This shift could be explained by the decrease in the LLS energy due to increased perturbation. However, maybe the more interesting observation is the difference between interfaces: while interface 6 shows only the shift in peak, interface 1 exhibits strong decrease in gain. By investigating the band structure (Fig. 18) we observe that ULS and injector wavefunctions are almost equal to zero at the interface 6, while at the interface 1 the values are higher. This is the reason that leads to the stronger leakage of electrons from the ULS to the LLS at the interface 1.

The large separation energy between the upper pair and the lower pair of bands leads to the difference in response when η or λ are increased. It can be noted that gain decreases much stronger for increased η. The reason for this behaviour is explained in Sec. 3.4: the increase in η enhances the scattering over all q values, while the increase in λ increase only the low momentum transfer scattering; and higher momentum scattering is more important for scattering between bands separated by large separation energy.

We must note, that it is estimated in Ref. [19], that leakage current from ULS to higher sub-bands is the most important mechanism of the interface roughness scattering on the QCL. However, our simulation does not show a significant increase in the higher band occupation. This could be due to the E_{typ} approximation used in the program.

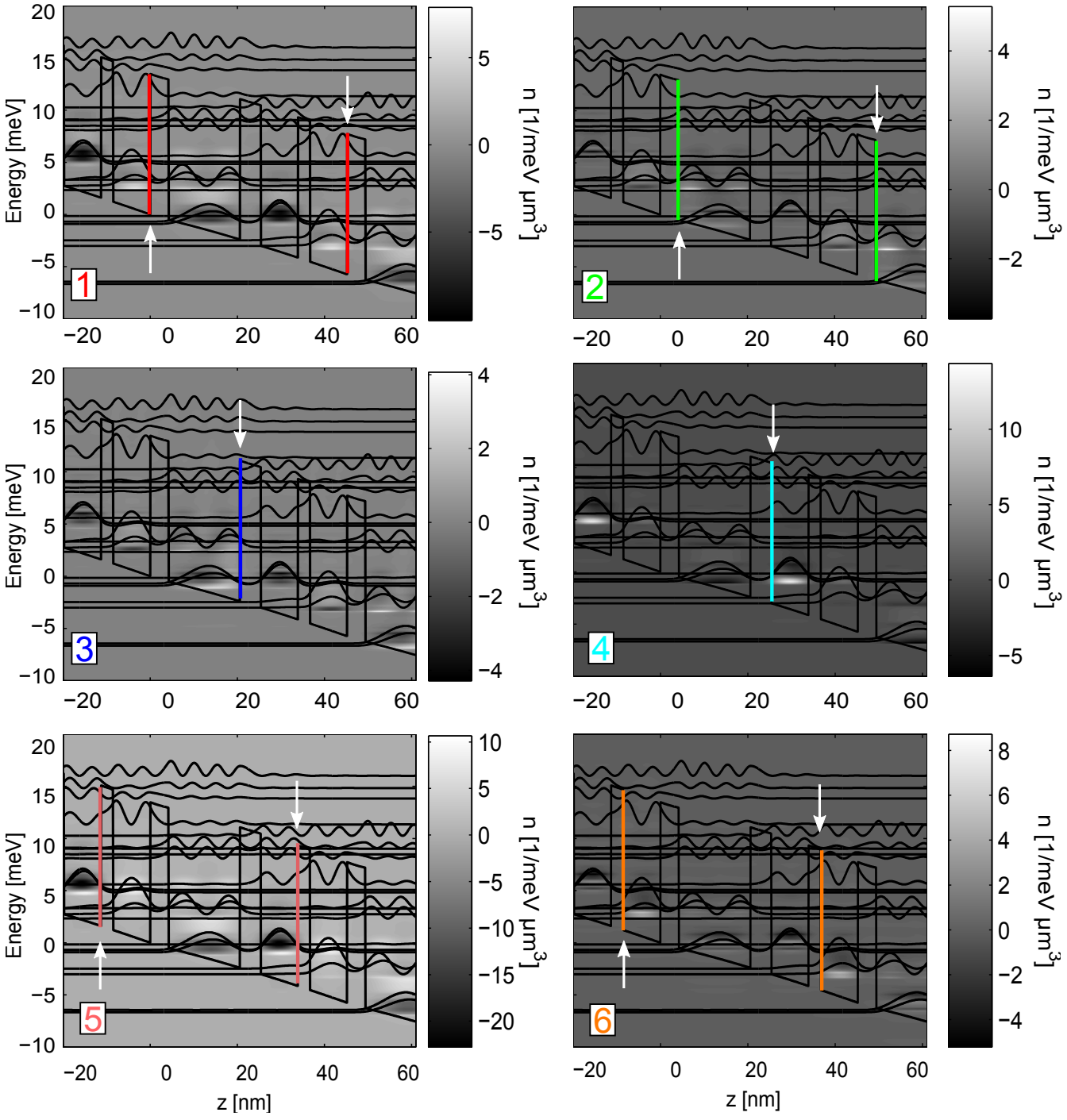

Figure 20: Relative density resolved in energy and growth direction (compared with reference) for six different positions of interface with increased η. Positions of altered interfaces are indicated by coloured lines (influence for corresponding interfaces is shown in Fig. 19). Bias per period is equal to 57.5 mV.

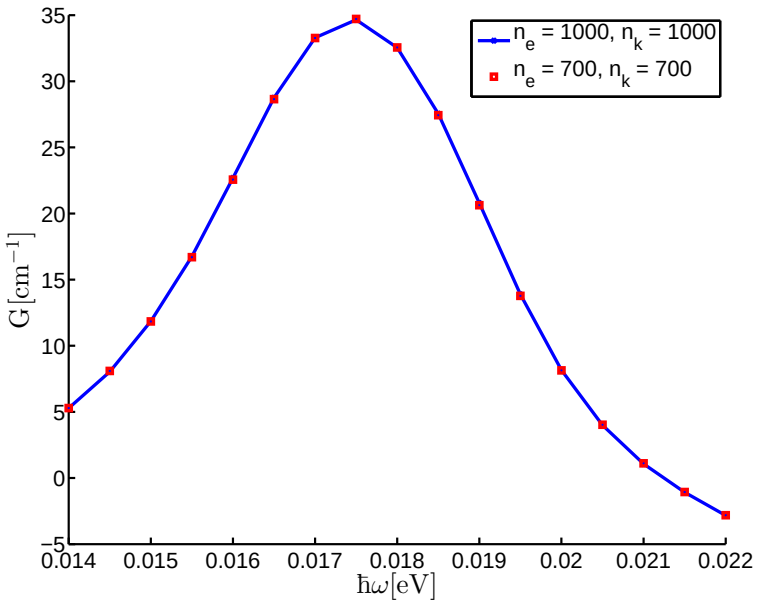

Figure 21: Convergence check for three-well laser. The difference in results with two different sets of precision defining parameters is negligible.

4.6 Convergence check

The convergence of simulations for three-well laser was investigated in order to determine the reliability of results. As described in Sec. 4.2, three parameters determine the precision of simulations. For this QCL, just as for two-well laser, values of $n_e = 700$, $n_k = 700$ and $\delta_{\text{konv}} = 5 \cdot 10^{-4}$ were used for all simulations. To check the validity of the results, a single simulation with increased parameters ($n_e = 1000$, $n_k = 1000$ and $\delta_{\text{konv}} = 1 \cdot 10^{-4}$) was used.

Gain in same range was calculated for different sets of parameters. The comparison is shown in Fig. 21. It is clear that there is no difference in results. Therefore it can be stated that results are well converged and valid.

5 Conclusion

In this work the influence of interface roughness was investigated. Two quantum cascade laser designs were considered in detail (the two-well laser documented in Ref [4] and the three-well laser documented in Ref. [5]). The QCLs were simulated using a program employing the non-equilibriums Green's function theory (Ref. [3]). The obtained results were analysed using theoretical treatment of possible elastic scattering events and also taking into account the model used in the program.

The distribution of electrons is changed due to the interface roughness scattering which can result in different effects on the laser behaviour. Both the current density dependence on bias and the gain spectrum changes. The main effect on the current density is an increase with increasing interface roughness scattering. Electrons spending less time in each sub-band can be the reason for this observation. Another studied effect is the additive influence (superposition) of different interfaces on current density. The change in current density that arises from the increase in IFR at a single interface is due to the change of electrons in sub-bands. However, the occupation changes by relatively small amount, therefore the total effect of several interfaces will be the sum of single interface effects.

Two effects were observed in the gain spectrum during the simulations: shift in the gain peak and a decrease in gain. The gain peak can either shift towards lower energies (red shift) or towards higher energies (blue shift). The explanations for this behaviour is the change in band structure due to the real part of self-energies.

The analysis suggests that interface roughness is an important scattering mechanism that can affect the performance of a laser. It influences the operation of laser mostly through scattering to the other bands of the same well, followed by the electron relaxation by the emission of phonons. Due to this effect the gain in the QCL is lowered, since electrons escape through leakage current. This process is of importance at the interfaces where the wavefunctions of sub-bands have high values and the large separation in energy.

It can be seen that the interfaces at lower potential energy side affect the operation of the QCL more. This could be important when growing these devices, since it is usually the case, that IFR depends on growth direction, as seen in [2].

6 Outlook

The main results of this work are the estimation of how the main leakage mechanism the interface roughness scattering affects the operation of quantum cascade lasers. The leakage of electrons to the lower energy sub-bands followed by relaxation of electrons was observed to happen. Another observed phenomenon is the change in the real part of the self-energies that affects the energy of sub-bands. The main effect of this phenomena is the redistribution of electrons in the sub-bands that leads to the changes in the current density and gain spectrum.

The study is not conclusive because not all observed results can be explained by these mechanisms. Another problem is that the used model simplifies the electron scattering from a sub-band to the single energy. Future study should focus on isolating the cause of observed shifts in the gain spectrum as well as further investigating the dominant effects of interface roughness.

Furthermore, this work investigated only two terahertz quantum cascade lasers. Additional structures should be analysed to expand the understanding of IFR to the wider range of devices, particularly to the mid-infrared lasers. This could lead to better understanding of the phenomenon, because the mid-infrared lasers tend to have different separation energies between the sub-bands then the terahertz QCL.

Ultimately, the understanding of interface roughness scattering could lead to the improved designs of quantum cascade lasers. Hypothetically, this could be achieved by designing the band structure to avoid leakage at the important sections of the QCL (*e.g.* between an upper lasing state and a lower lasing state).

A Simulation data

The following tables contains the parameters used in simulations. The displayed parameters describe technical data. The percentage of aluminium (Al) interchanged with gallium (Ga) in aluminium gallium arsenide ($Al_{1-x}Ga_xAs$) is denoted as x. The couple of parameters, that depend on x are also shown: conduction band offset ΔE_c and barrier effective mass m^*. These parameters were calculated using equations provided in Ref. [18]. Some other parameters are also shown: sheet doping density n_c and number of periods N (laser design parameters) as well as interface roughness parameters: average displacement η and average interface correlation length λ.

Table 7: Two-well laser. Ref. [4]

symbol	value
x	0.15
ΔE_c	0.1347 eV
m^*	0.067
n_c	1.5×10^{10} cm^{-2}
N	220
η_{ref}	0.15 nm
λ_{ref}	10 nm

Table 8: Three-well laser. Ref. [5]

symbol	value
x	0.15
ΔE_c	0.1347 eV
m^*	0.067
n_c	3.0×10^{10} cm^{-2}
N	222
η_{ref}	0.20 nm
λ_{ref}	10 nm

Glossary

e Extractor state.

i Injector state.

i-e Injector-extractor state.

IFR Interface roughness.

LLS Lower lasing state.

LO-phonons Longitudinal optical phonons.

MBE Molecular beam epitaxy.

MOCVD Metal organic chemical vapour deposition.

NEGFT Non-equilibrium Green's function theory.

QCL Quantum cascade laser.

RMS Root mean square.

ULS Upper lasing state.

References

[1] J. Faist, F. Capasso, D.L. Sivco, C. Sirtori, A.L. Hutchinson, A.Y. Cho, Science (New York, N.Y.) **264**(5158), 553 (1994)

[2] C. Deutsch, H. Detz, T. Zederbauer, A.M. Andrews, P. Klang, T. Kubis, G. Klimeck, M.E. Schuster, W. Schrenk, G. Strasser, K. Unterrainer, Optics express **21**(6), 7209 (2013)

[3] A. Wacker, M. Lindskog, D.O. Winge, IEEE Journal of Selected Topics in Quantum Electronics **19**(5), 1 (2013)

[4] G. Scalari, M.I. Amanti, C. Walther, R. Terazzi, M. Beck, J. Faist, Optics Express **18**(8), 8043 (2010)

[5] S. Kumar, Q. Hu, J.L. Reno, Applied Physics Letters **94**(13), 131105 (2009)

[6] R. Kazarinov, R. Suris, Sov. Phys. Semicond. **5**, 707 (1971)

[7] B.S. Williams, Nature Photonics **1**(9), 517 (2007)

[8] R. Köhler, A. Tredicucci, F. Beltram, H.E. Beere, E.H. Linfield, a.G. Davies, D.a. Ritchie, R.C. Iotti, F. Rossi, Nature **417**(6885), 156 (2002)

[9] B.S. Williams, H. Callebaut, S. Kumar, Q. Hu, J.L. Reno, Applied Physics Letters **82**(7), 1015 (2003)

[10] A. Cho, J. Arthur, Progress in Solid State Chemistry **10**, 157 (1975)

[11] E. Linfield, MBE growth of GaAs-AlGaAs terahertz frequency quantum cascade lasers (2014). IQCLW 2014

[12] J.L. Zilko, in *Handbook of Thin Film Deposition Processes and Techniques*, ed. by K. Seshan, second edition edn. (William Andrew Publishing/Noyes, 2002)

[13] J. Faist, *Quantum Cascade Lasers* (Oxford University Press, Oxford, 2013)

[14] S.C. Lee, A. Wacker, Physical Review B **66**(24), 245314 (2002)

[15] M. Lindskog, Analysis and optimisation of quantum cascade structures. Master thesis, Lund University (2012)

[16] A. Wacker. Negft-program manual

[17] C. Deutsch, A. Benz, H. Detz, P. Klang, M. Nobile, A.M. Andrews, W. Schrenk, T. Kubis, P. Vogl, G. Strasser, K. Unterrainer, Applied Physics Letters **97**(26), 261110 (2010)

[18] J.H. Davies, *The Physics of Low-dimensional Semiconductors* (Cambridge University Press, Cambridge, 1998)

[19] Y.V. Flores, S.S. Kurlov, M. Elagin, M.P. Semtsiv, W.T. Masselink, Applied Physics Letters **103**(16), 161102 (2013)